Actin-based propulsion of a microswimmer

A. M. Leshansky*
Department of Chemical Engineering, Technion-IIT, Haifa, 32000, Israel
(Received 11 April 2006; published 21 July 2006)

A simple hydrodynamic model of actin-based propulsion of microparticles in dilute cell-free cytoplasmic extracts is presented. Under the basic assumption that actin polymerization at the particle surface acts as a force dipole, pushing apart the load and the free (nonanchored) actin tail, the propulsive velocity of the microparticle is determined as a function of the tail length, porosity, and particle shape. The anticipated velocities of the cargo displacement and the rearward motion of the tail are in good agreement with recently reported results of biomimetic experiments. A more detailed analysis of the particle-tail hydrodynamic interaction is presented and compared to the prediction of the simplified model.

DOI: 10.1103/PhysRevE.74.012901 PACS number(s): 87.17.Jj, 47.63.Gd, 83.10.−y, 47.63.mf

Actin polymerization is a basic factor in the motility of many bacterial pathogens, such as *Listeria* or *Rickettsia* [1]. Recently proposed biomimetic systems have provided a significant advance in the study of actin-based propulsion and are considered as model systems for understanding motile functions involving actin polymerization. In these experiments, the bacteria are replaced by either polystyrene beads [2–5], phospholipid vesicles, or oil drops [6] covered with a variety of actin polymerization promoters. These microparticles being submerged into cell-free cytoplasmic extracts closely mimic the natural phenomena of actin tail formation and self-locomotion: (i) the polymerizing actin forms a cloud around the object and over a certain period of time becomes transformed into a cylindrical comet tail consisting of a meshwork of cross-linked filaments; (ii) the object is pushed forward by the comet tail which continues to elongate by polymerization at the particle surface. While biochemical aspects of actin nucleation and filament growth in this form of actin-based movement are now well understood [7], the underlying biophysical mechanism of the propulsive force is still under debate [8]. There are two leading biophysical models of actin-based propulsion. The elastic propulsion model [9] proposes that relaxation of the elastic stresses in actin gels growing on curved surfaces yields the propulsive force; the "tethered" Brownian ratchet model [10] assumes that the free tips of the polymerizing filaments hitting on the load surface due to thermal fluctuations provide the required propulsive thrust, while some filaments are transiently attached to the surface, opposing (and stabilizing) the motion. Recent experiments of [5] showed that actin polymerization on flat surfaces can also provide an efficient propulsive force. Moreover, they observed that flattened microdisks move faster than the spheres from which they were made. This suggests that curvature-dependent elastic stresses and actin gel deformation are, probably, not central for locomotion. Also, the sharply curved force-velocity relationship probed experimentally in [11] compares favorably with the prediction of the tethered ratchet model [10].

When the actin tail is anchored to the coverslip or cross linked into the host cell cytoplasm, the addition of new actin monomers at the cargo surface propels the load forward, whereas the tail remains stationary [12]. In this case, given that the comet tail is rigid enough, the propulsion velocity was assumed to be equal to the velocity of actin polymerization at the particle surface [10]. Since the forces associated with the filament attachment and dissociation (in the nano- to piconewton range) are usually several orders of magnitude higher than the viscous drag exerted on the particle by the extract fluid [4], hydrodynamic forces are neglected in the analysis of propulsion [10]. In dilute cell-free extracts the propulsion of a biomimetic cargo is often accompanied by a considerable retrograde displacement of the comet [3,5]. This observation suggests that in these experiments the actin tail was not anchored while still capable of pushing the load.

In this Brief Report the mechanism of propulsion in dilute extracts powered by the mobile actin tails will be addressed. In some sense, the problem of bead locomotion powered by the elongating actin tail, attached to its surface at one end and free at the other end, is analogous to the classical low-Reynolds-number microswimmer problem, though in the present case the swimming technique does not involve time-periodic shape strokes [13] or traveling surface waves [14], but rather based on a continuous "flow" of the filamentous tail due to actin treadmilling.

To estimate the velocity of the bead propulsion and the velocity of the tail compared to the mean polymerization velocity, I will develop a simple hydrodynamic model. The working hypothesis is that the mean rate of comet tail elongation at the interface between the bead and the tail, $\bar{v}_p$, is determined by the microscopic force balance of filament attachment and dissociation [10], particle shape [5], and elastic stresses in the growing tail [8] and is not affected by the macroscopic hydrodynamics. It is consistent with experimental observations [11], where the extract viscosity was shown to be a minor determinant of the propulsion speed: while the viscosity spanned a 500-fold range, bacteria were only slowed by a factor of ~20. Therefore, intercalation of actin monomers at the particle-tail interface pushes the mobile tail and the particle apart from each other with the net rate of $\bar{v}_p$ [3]. Since the freely suspended particle-tail assemblage should generate a force-free flow field, the viscous load on the actin comet and on the particle should compensate each other, $\mathbf{F}_p \approx -\mathbf{F}_c$, i.e., actin polymerization at the interface be-

*Electronic address: lisha@tx.technion.ac.il

 ©2006 The American Physical Society

tween the bead and the tail acts locally as a force dipole or stresslet. I further assume that the friction force exerted on the actin comet tail is well approximated by the viscous drag on a porous cylinder (prolate porous spheroid). Neglecting the particle-tail hydrodynamic interaction one can write that

$$\lambda\mu(\ell/2)E(\bar{v}_p - u) \approx S\mu a u, \tag{1}$$

where u is the velocity of the particle, a is the typical particle size, λ is the permeability or shape factor of the tail, S is the particle shape factor, μ is the viscosity of the dilute cell-free extract, and $E=(\ln 2/\epsilon-0.5)^{-1}$ with $\epsilon=d/\ell$ being the ratio of the comet diameter d to its length ℓ. Here λ is generally a function of permeability of the filamentous actin tail, k, and its length, ϵ, and is anticipated to range between zero for a highly porous tail and 4π corresponding to the impermeable rod [15].

Given the mean polymerization velocity $\bar{v}_p$ the velocity of the tail in the laboratory frame is given just by $u_c=\bar{v}_p-u$. Thus, it follows from (1) that for long tails, $\epsilon \ll 1$, the particle and the comet velocities can be found as

$$u \simeq \bar{v}_p\left(1+\frac{S}{\lambda}\epsilon \ln 1/\epsilon\right)^{-1}. \tag{2}$$

Here it is assumed that the comet diameter $d \approx 2a$ and thus $a/\ell \simeq \epsilon/2$. It is readily seen from (2) that from the fluid-mechanical point of view the effective propulsion requires long and dense actin tails. Indeed, for $\epsilon \ll 1$ and $S/\lambda \sim O(1)$, the velocity of the particle asymptotes to the mean polymerization velocity, $u \simeq \bar{v}_p$, while the velocity of the retrograde tail motion is small, $u_c=O(\epsilon \ln \epsilon^{-1})$. In experiments, however, a considerable retrograde motion of the tail was observed [3]. Given that in the experiments the actin density in the tail may vary significantly, we consider rather wide range of permeability, $k=(6-30)\times 10^{-4}$ μm^2. The radii of the actin filaments are $b \sim 4$ nm and this translates into the dimensionless permeability $\kappa^*=k/b^2 \simeq 31.2-187.5$ or into the hydrodynamic resistance $\alpha^*=1/\sqrt{\kappa^*} \simeq 0.073-0.16$.

The relation between the uniform concentration of obstructions, c, and α^* for a viscous flow through an array of randomly scattered cylinders in an arbitrary orientation is given by $c=\frac{\zeta(\zeta+4)}{6(\zeta+2)}$, where $\zeta=\alpha^*\frac{K_0(\alpha^*)}{K_1(\alpha^*)}$ with K_i being the modified Bessel functions of the second kind [16]. Thus, the filament content in the gel can be estimated as $c \simeq 0.018-0.005$. The average separation between the filaments in the comet can be estimated via the use of the cell model [17] as $\Delta/b \simeq 2(c^{-1/2}-1)$ yielding $\Delta \sim 52-106$ nm which is in the range of interfilament spacing corresponding to a loose actin meshwork cross linked by filamin [7]. Since actin gel is sparse enough ($c<0.3$) we can approximate the drag force exerted on the comet tail by that applied on a prolate porous spheroid using Brinkman's effective medium approach [18]. Also, for low permeability of the actin comet, $\kappa=k/a^2 \to 0$, the Darcy approximation is often considered appropriate [19]. The viscous drag force exerted on the comet tail is calculated via the use of prolate spheroidal coordinates for both models (see Fig. 1). As expected, in the vicinity of $\kappa=0$ both models yield the same asymptotic result

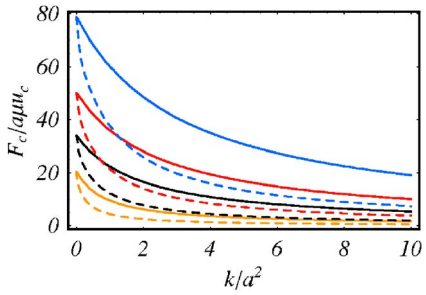

FIG. 1. (Color online) The scaled drag force $F_c/a\mu u_c$ on porous prolate spheroid vs the scaled permeability $\kappa=k/a^2$, calculated for different values of the semifocal distance c: $c=1$ (yellow, lower lines), 5 (black), 10 (red), and 20 (blue, upper lines), from bottom to top. The solid and the dashed lines correspond to the Darcy and Brinkman aproximations, respectively.

corresponding to an impermeable rigid rode as $F_c/a\mu u_c$ scales like $(\epsilon \ln 1/\epsilon)^{-1}$ for $\epsilon \ll 1$. Since $\kappa=\kappa^*(b/a)^2$ for particles with $a=0.1-1$ μm [3] it follows that κ varies between 5×10^{-4} and 0.25.

Once F_c is computed one can calculate the velocity of the cargo via (1) or (2). Note that for the Darcy model [19] the permeability factor can be found in a closed form as $\lambda=4\pi/(1+\kappa E)$. For a rigid sphere ($S=6\pi$) the dimensionless propulsion speed $u/\bar{v}_p$ is plotted in Fig. 2 vs κ (a) and vs ϵ (b). An important observation is that the velocity dependence on permeability in the vicinity of $\kappa=0$ is quite weak and as κ increases from 0 (impermeable) to 0.2, the propulsion is only slowed by a factor of ~ 1.3 as ϵ varies from 0.05 to 0.2. The longer the tail, the weaker the dependence on κ, since for $\ln 1/\epsilon \gg \kappa$ it follows that $\lambda \sim 4\pi$. However, the velocity dependence on the tail length is quite appreciable, as can be seen in Fig. 2(b). The forward motion of micrometer-

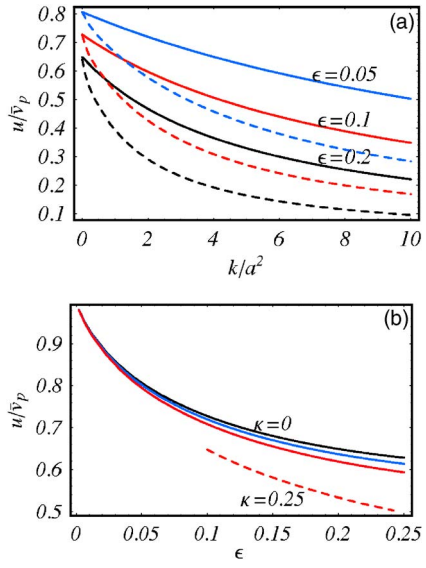

FIG. 2. (Color online) Scaled propulsion velocity of the bead. The solid and dashed lines correspond to the Darcy and Brinkman approximations, respectively. (a) $u/\bar{v}_p$ vs scaled permeability κ for various reciprocal comet lengths $\epsilon=d/\ell$; (b) $u/\bar{v}_p$ vs ϵ, for $\kappa=0$ (black), 0.1 (blue), 0.25 (red).

diameter beads with $u\sim 0.3$ μm/min vs the rearward displacement of the tail with the rate of $u_c\sim 0.2$ μm/min reported in [3], which translates into $u/\bar{v}_p\sim 0.6$, can be readily explained by the present theory.

To address the efficiency of the motility mechanism powered by actin polymerization it is necessary to estimate the power expended in swimming. Several definitions of the hydrodynamic efficiency have been proposed [13]. I follow the definition $\delta=S\mu a u^2/\mathcal{P}$, where $\mathcal{P}$ is the energy dissipated in swimming with velocity u, and the expression in the denominator is the work expended by dragging of the particle with velocity u by an external force. Neglecting viscous dissipation within the porous tail, the power expended in actin-based propulsion can be estimated as $\mathcal{P}\geqslant -\int_s \boldsymbol{n}\cdot\boldsymbol{\sigma}\cdot\boldsymbol{v}\, ds \sim F_p(u+u_c)=Sa\mu u\bar{v}_p$. Thus the upper bound on the swimming efficiency coincides with the velocity ratio $\delta\leqslant u/\bar{v}_p<1$. Obviously, self-locomotion powered by polymerizing actin tails is quite efficient as $u/\bar{v}_p>50\%$ even for sparse tails with $\kappa\sim 0.25$ and moderate lengths $\epsilon<0.25$ (see Fig. 2 for $S=6\pi$). For comparison, the swimming efficiency for cyanobacteria self-propelled by traveling tangential surface waves is expected to be less than 1% and the efficiency of the bacterial flagella is only about 2% [14]. The high hydrodynamic efficiency of the actin-based swimming reflects the simple fact that the continuous actin treadmilling in the tail is aligned with the direction of propulsion and no mechanical work is wasted on reverse or transverse movements.

When hydrodynamic interaction between the bead and the tail is neglected it has been assumed that $F_p\approx F_c=\mathcal{F}_c\ell$, with $\mathcal{F}_c\approx\lambda\mu(E/2)u_c$ being the constant force density of the line distribution of Stokeslets along the central line of the straight comet tail [15]. To estimate the effect of hydrodynamic interaction (screening) between the tail and the bead I assume that the flow is generated by the distribution of $\mathcal{N}$ Stokeslets of strengths $f_c=\mathcal{F}_c\ell/\mathcal{N}$ along the comet center line (the higher-order singularities such as Stokes dipoles and quadrupoles are probably not necessary if $\ell\gg a$) in the vicinity of the mobile spherical bead. The flow due to a Stokeslet of strength $\boldsymbol{f}_c$ acting at $\boldsymbol{x}_2$ in the vicinity of the rigid sphere of radius a centered at $\boldsymbol{x}_1$ and separated by $R=|\boldsymbol{x}_2-\boldsymbol{x}_1|/a$ (the distance is scaled with the particle radius a) can be written as

$$\boldsymbol{v}=\boldsymbol{f}_c\cdot\boldsymbol{\mathcal{G}}(\boldsymbol{x}-\boldsymbol{x}_2)/8\pi\mu+\boldsymbol{v}^* -\boldsymbol{f}_p\cdot\left(1+\frac{a^2}{6}\nabla^2\right)\boldsymbol{\mathcal{G}}(\boldsymbol{x}-\boldsymbol{x}_1)/(8\pi\mu). \tag{3}$$

Here $\boldsymbol{\mathcal{G}}$ is the Oseen tensor, $\boldsymbol{v}^*$ is the image field of the Stokeslet near a stationary sphere, and the last term corresponds to a translation of the sphere with $\boldsymbol{f}_p$ being the viscous drag force exerted by the translating particle. It can be shown that $\boldsymbol{v}^*$ can be written as a multipole expansion around the sphere center $\boldsymbol{x}_1$ [15] and to the lowest order it is given by

$$\boldsymbol{v}^*\simeq -\boldsymbol{f}_c\cdot\left[\left(\frac{3}{2R}-\frac{1}{2R^3}\right)\boldsymbol{dd} +\left(\frac{3}{4R}+\frac{1}{4R^3}\right)(\boldsymbol{I}-\boldsymbol{dd})\right]\cdot\mathcal{G}(\boldsymbol{x}-\boldsymbol{x}_1)/(8\pi\mu).$$

Of course, as the Stokeslet is placed nearer to the sphere, the contribution from the higher-order singularities becomes important [20] but since we are not interested in the details of the flow in the vicinity of the particle-tail interface, the lowest-order representation will be sufficient. The force $\boldsymbol{f}_p$ counterbalancing $-\boldsymbol{f}_c$ is screened by the hydrodynamic interaction with the particle surface due to $\boldsymbol{v}^*$. Taking into account that $\boldsymbol{v}$ in (3) generates a force-free flow at infinity, $\boldsymbol{f}_p$ can be readily related to $\boldsymbol{f}_c$ as

$$\boldsymbol{f}_p=\boldsymbol{f}_c\cdot\left[-\boldsymbol{I}+\left(\frac{3}{2R}-\frac{1}{2R^3}\right)\boldsymbol{dd} +\left(\frac{3}{4R}+\frac{1}{4R^3}\right)(\boldsymbol{I}-\boldsymbol{dd})\right]. \tag{4}$$

The force $\boldsymbol{f}_p$ vanishes as the Stokeslet moves to the particle surface due to hydrodynamic screening, and it asymptotes to $-\boldsymbol{f}_c$ for $R\gg 1$. Therefore, the propulsion powered by short tails is even less efficient than that predicted by the simplified theory (1) since some of the forcing due to polymerization is screened by the flow $\boldsymbol{v}^*$. The common experimental observation is that initially the nonmotile particle is surrounded by the compact actin cloud and it eventually becomes motile, as the cloud transforms into a tail [2,3,5]. Equation (4) also suggests that the lower portion of the tail should play an important role in propulsion. The self-locomotion of microdisks observed in [5] provides strong evidence in favor of this argument. In these experiments the microdisks with double-face tails move edge-on with the lower portion of both their tails being aligned with the direction of propulsion, and it was argued that "the assembly is pushed by the lower tail in the direction normal to the disk face it contacts."

To quantify the overall effect of the hydrodynamic screening for long tails I next consider, for the sake of simplicity, the straight portion of the actin tail with $\boldsymbol{f}_p^{\parallel}$ being a force density distributed along the comet central line. The thrust on a microsphere powered by a straight actin comet tail, F_p, can be determined by summing up contributions from $\mathcal{N}$ Stokeslets, i.e., integrating (4) over R from 1 to $\ell/a=2\epsilon^{-1}$, and for, $\ell\gg a$, the compact asymptotic result can be readily derived,

$$F_p=\mathcal{F}_c\ell\left(1+\frac{3}{4}\epsilon\ln\epsilon+O(\epsilon)\right). \tag{5}$$

This indicates that the error due to the assumption of uniform force density per comet unit length, i.e., $F_p\approx\mathcal{F}_c\ell$ in (1), is

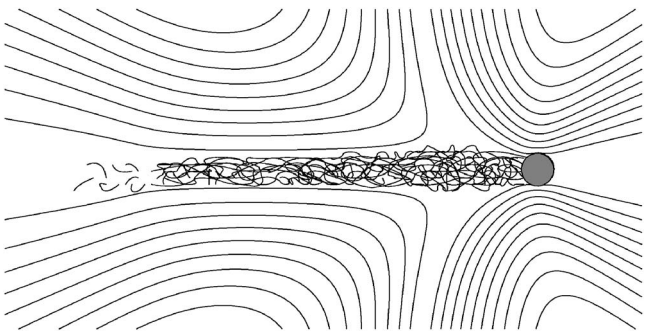

FIG. 3. The streamline flow pattern around a microbead (gray circle) propelled by the polymerizing actin tail.

$O(\epsilon \ln \epsilon)$ and hydrodynamic screening is not significant for long tails, $\epsilon \ll 1$. When the $O(\epsilon \ln \epsilon)$ term in (5) is considered in the derivation of (2), the scaled propulsion velocity of the bead, $u/\bar{v}_p$, diminishes by the value of $3S/4\lambda(\epsilon \ln \epsilon)^2$ due to hydrodynamic screening. This reduction is less than 10% of the value computed in (2) for tails with $\epsilon \leqslant 0.15$ and $\kappa \leqslant 0.25$ when the Darcy model for λ is used.

The typical streamline pattern around a moving spherical bead propelled by an elongating actin tail is depicted in Fig. 3. The velocity field, which takes into account hydrodynamic screening, is calculated by superimposing the solution for rearward translation of the Brinkman prolate spheroid on that for the forward translation of a rigid sphere corrected by one reflection [15] to satisfy approximately the velocity boundary conditions on the tail and the particle boundaries.

In conclusion, I have developed a simple hydrodynamic model of microswimmer propulsion induced by actin polymerization at the particle surface. The predicted velocities of the cargo propulsion and the retrograde motion of the actin comet tail compare favorably with previously reported experimental results. Some estimates regarding the dependence of the propulsion speed on filament density (i.e., tail porosity) and comet tail length are obtained. The upper bound on the swimming efficiency demonstrates that actin-based propulsion is superior to other motility mechanisms.

I would like to thank A. Mogilner, J. Avron, D. Broday, and O. Gat for stimulating discussions on the subject and T. Zlatanovki for sharing the MATHEMATICA subroutine for calculation of the viscous drag on a prolate Brinkman spheroid.

[1] E. Gouin, M. D. Welch, and P. Cossart, Curr. Opin. Microbiol. **8**, 35 (2005).
[2] L. Cameron *et al.*, Proc. Natl. Acad. Sci. U.S.A. **96**, 4908 (2000); A. Bernheim-Groswasser *et al.*, Nature (London) **417**, 308 (2002); J. Plastino, S. Olivier, and C. Sykes, Curr. Biol. **14**, 1766 (2004).
[3] L. A. Cameron *et al.*, Mol. Biol. Cell **15**, 2312 (2004).
[4] Y. Marcy *et al.*, Proc. Natl. Acad. Sci. U.S.A. **101**, 5992 (2004); J. L. McGrath *et al.*, Curr. Biol. **13**, 329 (2003).
[5] I. M. Schwartz *et al.*, Curr. Biol. **14**, 1094 (2004).
[6] A. Upadhyaya *et al.*, Proc. Natl. Acad. Sci. U.S.A. **100**, 4521 (2003); H. Boukellal *et al.*, Phys. Rev. E **69**, 061906 (2004).
[7] T. Pollard, L. Blanchoin, and R. Mullins, Annu. Rev. Biophys. Biomol. Struct. **29**, 545 (2000).
[8] J. Plastino and C. Sykes, Curr. Opin. Cell Biol. **17**, 62 (2005); A. Upadhyaya and A. Oudenaarden, Curr. Biol. **14**, 467 (2004).
[9] F. Gerbal *et al.*, Biophys. J. **79**, 2259 (2000).
[10] A. Mogilner and G. Oster, Biophys. J. **84**, 1591 (2003).
[11] J. L. McGrath *et al.*, Curr. Biol. **13**, 329 (2003).
[12] J. A. Theriot *et al.*, Nature (London) **357**, 257 (1992); L. Cameron *et al.*, Proc. Natl. Acad. Sci. U.S.A. **96**, 4908 (1999).
[13] A. Shapere and F. Wilczek, J. Fluid Mech. **198**, 557 (1989); J. E. Avron, O. Gat, and O. Kenneth, Phys. Rev. Lett. **93**, 186001–1 (2004); A. Najafi and R. Golestanian, Phys. Rev. E **69**, 062901 (2004); J. E. Avron, O. Kenneth, and D. H. Oaknin, New J. Phys. **7**, 234 (2005).
[14] K. M. Ehlers *et al.*, Proc. Natl. Acad. Sci. U.S.A. **93**, 8340 (1996); H. A. Stone and A. D. T. Samuel, Phys. Rev. Lett. **77**, 4102 (1996).
[15] S. Kim and S. J. Karrila, *Microhydrodynamics* (Butterworth-Heinemann, Boston, 1991).
[16] D. M. Broday, Bull. Math. Biol. **64**, 531 (2002).
[17] J. Happel, AIChE J. **5**, 174 (1959).
[18] T. Zlatanovski, Q. J. Mech. Appl. Math. **52**, 111 (1999); **53**, 173(E) (2000).
[19] P. Vainshtein, M. Shapiro, and C. Gutfinger, Int. J. Multiphase Flow **28**, 1945 (2002).
[20] The velocity field $\boldsymbol{v}^*$ can be alternatively represented by a line distribution of a small collection of low-order singularities along the segment that runs along the sphere-Stokeslet axis from the sphere center to the inverse point $\boldsymbol{x}_2^*$ defined as $|\boldsymbol{x}_2^* - \boldsymbol{x}_1| = (R/a)^{-1}$ [15].